Soft Matter

Soft Matter

www.rsc.org/softmatter

ROYAL SOCIETY OF CHEMISTRY

ROYAL SOCIETY OF CHEMISTRY

www.rsc.org/softmatter

Effect of Entrapped Phase on the Filling Characteristics of Closed End Nanopores

Chirodeep Bakli and Suman Chakraborty*

Department of Mechanical Engineering, Indian Institute of Technology Kharagpur, Kharagpur 721302, INDIA

1

We investigate the filling dynamics in closed-end capillaries of sub-micron length-scales, in which the displacing phase advances at the expense of the entrapped phase. Contrary to common intuitions, we reveal that the existence of a displaced phase in a closed end nano-scale system does not necessarily retard the meniscus advancement over all temporal regimes unlike what is observed in cases of macro-scale capillaries, but can also sometimes augment the local filling rates. We bring out the combined effect of surface wettability and the displaced phase molecules on the pinning-depinning of the meniscus and hence, on the local dynamics of capillary filling. We also employ a simple force balance based model to capture the essential interfacial phenomena governing this behavior, and benchmark the same with our molecular dynamics simulations. Our results suggest a possible mechanism of modifying the effective wettabilities of nano-scale capillaries, without any modification of the surface architecture or treating the surface chemically.

Introduction

Capillary flows are ubiquitous in not only in several natural phenomena but also find numerous applications in a varied spectrum of industrial processes. With diminishing length scales, the increasing surface area to volume ratio tends to make the surface forces dominate over bulk forces and hence, in the process aids capillarity. Thus, capillarity often becomes an effective mechanism of propelling fluids without the use of any external pressure gradients in conduits of micrometer and nanometer length scales[1,2]. The implications of capillary filling over small scales, therefore, are not surprisingly wide ranging, encompassing applications spanning from nanofluidic devices[3], porous nanomaterials[4], geophysics[5], enhanced oil recovery[6], to biomembranes[7].

Traditionally, in many of the above applications, the Lucas Washburn (LW) equation [8,9] captures the essential features of capillary filling dynamics, using a balance of viscous and surface tension forces. However, miniaturization induces certain extraneous factors to the classical LW description. Consequently, the phenomenon of capillarity and the associated motion of the three-phase contact line, over miniaturized scales, are considered to be profoundly affected by aspects like the substrate wettability[10–14], roughness[14–20], dynamic contact angle (DCA) [21–24], presence of ionic impurities [25–28] etc. In spite of these numerous investigations, the contact line motion, through the course of capillary imbibition, over miniaturized scales remains one of the least understood topics in the field of interface science. The contact line, which is formed at the junction of fluid(s) and the confining solid boundary, may primarily evolve with the movement of fluid with respect to a stationary solid and such examples occur in oil extraction[6], film spreading etc[29]. On the other hand, interfaces may also evolve as a solid moves in a stationary fluid pool such as in the case of a recording disk drive[30]. As opposed to the bulk fluid motion, the contact line dynamics with the no slip boundary condition poses a singularity[31] accompanied by a multi-valued behavior in the velocity. In macro-scale flows, this singularity is generally resolved by considering the fluid film moving over a thin film which instantaneously prewets the surface [32]. However, this assumption becomes questionable over reduced length scales. This may be attributed to the fact that below the micron regime, the molecular diffusion plays a significant role. Thus, the presumption of any film between the bulk fluid and solid

surface becomes empirical. Moreover, barring the cases of completely wettable substrates, rapid propagation of a prewetting film over partially wetting materials seems to be improbable.

Pertaining to the contact line motion in narrow capillaries mentioned as above, the effects of the displacing liquid medium as well as that of the solid substrate have been extensively discussed. However, insufficient insight has been available on the influence of an entrapped displaced phase in a closed end nano-capillary. Recently, a few research investigations have been focused to bring out the effects of an entrapped phase on capillary dynamics [33–41]. One important conclusion drawn from these studies is that the displaced phase would trivially retard the motion of the displacing fluid in a closed-end capillary, owing to increasing density of the entrapped molecules. However, possible extrapolation of the underlying considerations over capillaries of nanometer scales has not remained far from being questionable, and is yet to be comprehensively addressed.

Here, we attempt to bring out the implications of the displaced phase towards filling up of a closed end capillary of nanometer length scales. We show that the presence of the trapped phase does not necessarily slow down the meniscus movement in case of nano-scale capillaries. Rather, the meniscus speed may turn out to be a non-monotonous function of the extent of the displaced column being trapped. In effect, the meniscus marches by a complex process which combines molecular diffusion and evaporation-condensation at the contact line[42]. The pertinent interfacial phenomenon is grossly manifested as the alternate pinning-depinning of the meniscus. We demonstrate that the gas compression between the meniscus and the closed end may non-trivially affect this pinning-depinning of the contact line over nanoscopic scales (for a schematic depiction, see Fig. 1), and may either accelerate or retard the displacing fluid front depending on the concentration of the gas phase and the wettability of the substrate. Through molecular dynamics (MD) simulations, we obtain the conditions under which the displaced phase can impart pseudo lyophilicity to the substrate, despite an otherwise indicating intrinsic wettability. These results may help not only to comprehend the contact line dynamics in nanochannels in presence of a trapped gas in a better way, but also may facilitate in providing means of manipulating the 'effective' wettability of a substrate without chemically or physically modifying the same.
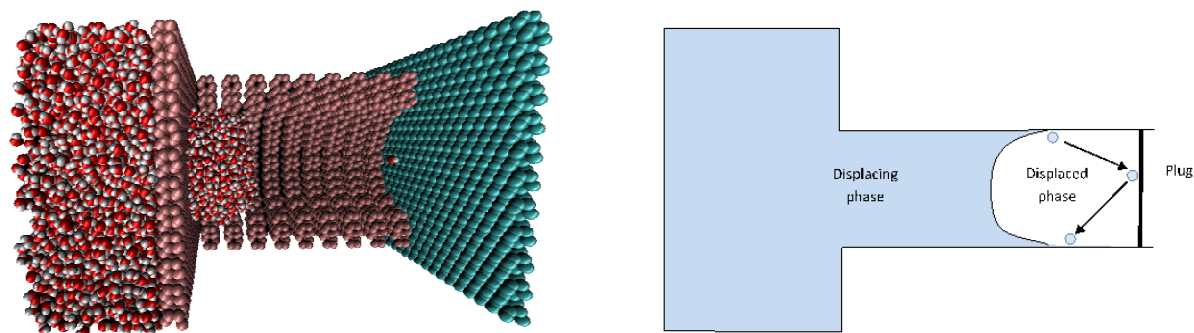
Figure 1. A MD snapshot of capillary filling in a closed pore (left). Molecules escape into gas phase from the bulk liquid and get trapped between the meniscus and plug. These trapped molecules shuttle between the plug and invading fluid front affecting the pinning-depinning of the meniscus. The cartoon (right) shows the extended meniscus and a representative case of water molecule getting reflected at the plug and altering the ambient conditions near the three-phase contact line.

MD Simulations

We consider a circular capillary pore attached to a large reservoir containing water molecules. The walls of the reservoir and the capillary are constituted of molecules in FCC lattice in <100> plane. The capillary pore forms a continuous crystal structure with the reservoir. The pore is obtained by removing the atoms within a radius of 2 nm. The reservoir contains 48204 water molecules in a dimension of $12 \times 12 \times 10$ nm. In a typical simulation for capillary filling, the set up is confined within a simulation box of comparatively larger dimensions, and the fluid molecules moving into the gas phase have quite a less probability to interact with the imbibing fluid, once these molecules leave the bulk. In order to simulate the identical physical conditions of a closed pore, we append an impermeable solid plug at the other end of the capillary pore, composed of the same material as that of capillary walls, and hence having the same intrinsic wettability. This arrangement traps the gas phase molecules in the system and these gradually get compressed between the imbibing liquid and the capillary plug. The setup attempts to mimic the conditions that exist in a natural closed-end capillary widely encountered in petroleum and shale-oil extraction. The wall atoms are allowed to vibrate about their equilibrium positions instead of

being rigid. This corresponds to a more physically realistic situation and removes the artifacts that may be incurred due to fixed walls[43]. The wall atoms are tethered to springs of sufficiently high spring constants so as to prevent vibrations over a threshold level[44]. The walls are thermostatted using Nose-Hoover thermostat at $300K$ and the fluid molecules are allowed to exchange heat via collisions with the flexible wall and hence maintain the temperature.

Water molecules are modeled using the SPC/E model[45]. We initially arrange the water molecules in a regular lattice by defining the three coordinates of each particle in a Cartesian coordinate system and then go for energy minimization of system. The process of energy minimization ensures that the liquid is in a random molten configuration to begin the actual simulations. The initial velocities are calculated using Maxwellian distribution at $300K$. At first, the system is equilibrated with a hypothetical impenetrable wall at the pore entrance and then equilibrated system is then allowed to evolve to build the vapor pressure in the pore with this hypothetical wall being removed and finally the imbibition simulation is conducted. The time integration of the equation is performed using leap-frog algorithm with the potentials of the individual particle described. The van der Waals interactions are accounted for by considering hetero-nuclear Lennard-Jones (LJ) interactions applied using standard mixing rules [46]. The wall molecules are chosen to be LJ particles. For the wall LJ parameters we choose, $\sigma_{ww} = 0.35nm$ and ε_{ww} is varied from $0.1 - 6kJ/mol$ to obtain variation of substrate wettability from hydrophobic to completely wettable capillary pores. The electrostatic interactions are accounted for using a particle-particle particle-mesh (PPPM) algorithm. For the simulations, we have chosen a van der Waals cut-off of 5σ. We select various capillary pore lengths as would be discussed later and the simulation time depends on the length of capillary to be filled. Typical simulations run for $2ns\left(2\times10^6 \text{ time steps}\right)$ and take about 50hours/ns of simulations on i7 processors. We use Leap-frog algorithm to numerically integrate the equations of motions and the size of time step chosen is 0.001ps. The data is averaged over 50 simulation runs to obtain statistically reliable and robust results.

The meniscus position is determined by tracking the imbibing fluid density along the capillary axis. The location where the density drops to half of the bulk density is considered to be the location of the meniscus[24]. We obtain the shape of the meniscus by binning the capillary pore

and hence, measure the contact angle. We divide the capillary into cylindrical shells with a size that is small enough to obtain the appropriate curvature shape without causing abrupt density fluctuations in the resulting profile. The curvature gives a qualitative idea about the contact angle of the liquid imbibing through the capillary. Contact angle, being a macroscopic quantity, does not have a true physical counterpart for a flow through nanochannel. However, in this work, one of our aims is to provide a blueprint for experimental systems and for oil extraction and other similar applications in the industrial paradigm where every parameter can be physically realized. Accordingly, we attempt to quantify the channel wettability (an intrinsic physical property that is embodied into the surface by virtue of its atomic arrangement) in terms of the contact angle (a macroscopic property that can be easily measured in experiments). In order to provide this unified representation, we measure the contact angles of sessile droplets on surfaces similar to the one used in the nanochannel by varying the Lennard-Jones potential parameter. Following this, we replicate the same interaction parameters for the particles constituting the walls of the nanochannel, and map the contact angle values obtained in the sessile drop simulation. This, in turn, defines the channel wettability in terms of the contact angle.

MD Results

We first consider several cases of closed end capillaries, with solid plugs being located at $x = 9, 12, 15 \ and \ 20 nm$ (the distances being measured from junction of the reservoir and capillary pore). All capillaries are considered to be perfectly wettable. A perfectly wettable capillary would have a thin film of the imbibing phase that moves ahead of the meniscus, and the bulk fluid moves on a prewetted surface. Thus, for wettable surfaces, the invading water front encounters an atomically smooth surface that intrinsically exhibits minimum contact angle hysteresis[15,47] . As we discuss later in the text, if a perfectly wettable pore demonstrates flow alteration caused by the plug, the partially wettable pores would be more likely to demonstrate similar behavior and possibly amplified. We plot the square of meniscus height versus time to represent the primary meniscus dynamics, as depicted in Fig. 2 ; the meniscus height being measured from the junction of the reservoir and the capillary pore. The initial filling rates for all the closed capillaries remain almost similar. As the meniscus hits the plug, the level plateaus at the plug height with small fluctuations. The meniscus hitting the plug, however, is only captured for the two shortest capillaries within the time frame chosen to plot the trends. A closer

observation of the plots yields an interesting trend; in each of the capillaries, before the menisci hit the plug, there occurs a temporal regime where the filling rate is larger than for the larger capillaries. For the plug placed at $l = 9nm$, the zone lies somewhere between $500 - 700\,ps$, where it can be easily observed that the blue (bold) line is above the other curves. In the case of $l = 12nm$, this 'take-off' zone lies somewhere between $800 - 1000\,ps$. For $l = 15nm$ and $l = 17nm$, the corresponding zone exists beyond $1500\,ps$. For the largest capillary, a similar zone exists which has been excluded from the displayed plot, in order to obtain a magnified view of the phenomenon occurring. Analyzing from a continuum based framework and referring to the reported macro-scale capillary filling studies [33,40], one would conclude that shorter capillaries should have shown a filling rate always lower than a larger capillary or at most equal. A shorter pore ensures faster gas compression between the meniscus and the plug, and hence is likely to exhibit a more pronounced effect of flow retardation owing to the viscosity of the displace phase. However, our preliminary findings seem to contradict this intuitive notion.
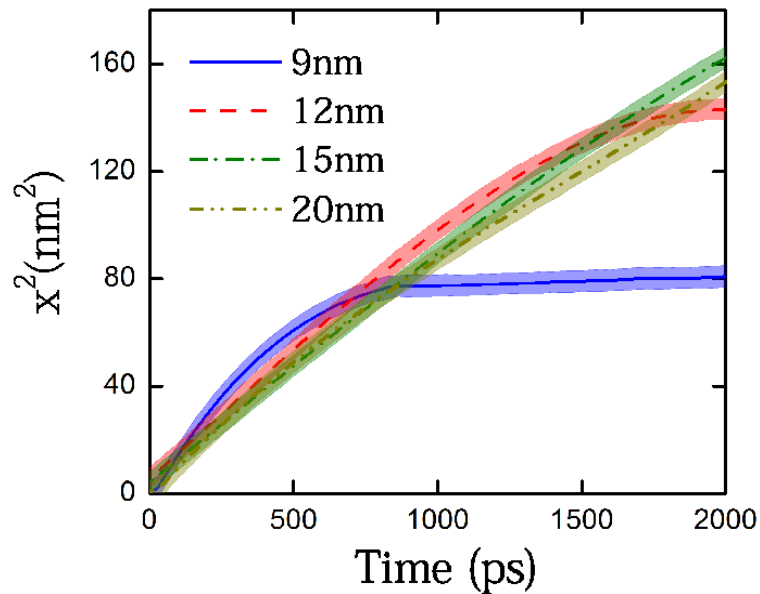
Figure 2. Comparison of filling rateof cpmpletely wettable closed capillaries with the plug placed at different locations. The plug is observed to first enhance and then retard the rate of filling as the meniscus approaches the plug. The square of meniscus height is as a function of time. This helps us to obtain a nearly straight-line plots (see the discussion on LW equation) which aids to visually compare the data. The error bars are shown using the shaded area in the plot.

Since, here we are more interested in the filling rates rather than the meniscus position; we try to directly compare the instantaneous filling rates, i.e. the local meniscus velocities for the capillaries of various lengths. If we presume that the plug height would induce velocity variation in the capillaries, then in that case plotting the velocities on the same time scale would not help in deciphering the trend. With the aim to circumvent this problem, we plot the velocities of these four completely wettable capillaries having different plug heights with respect to the meniscus height in Fig. 3 . This representation helps us to efficiently capture both the temporal march of the capillary front and the distance of the meniscus from the plug. The velocity profiles are smoothened to remove the statistical fluctuations so as to aid the eye towards capturing the trends in the evolving meniscus. The blue (bold) line for the shortest capillary has the maximum initial velocity, which gradually decays as the plug is approached and the trend finally reaches a plateau. Following this, one can also observe that the meniscus velocity assumes maximum values in orders of increasing plug heights. In the representative plot shown, the longest capillary is yet to reach the maxima (which occurs after 12nm). This unexplained increase in velocity at an intermediate distance from the plug has not been previously captured; the primary reason for this deficit being the macroscopic nature of the reported studies on the closed capillaries. The study we conduct here, as per our knowledge, is the first molecular level investigation conducted for imbibition in closed capillary pores and this can be attributed to the unprecedented results observed. We will make an endeavor to explain these trends in our subsequent discussions. Towards that, we will also bring out a non-trivial contribution of the intrinsic contact angle, which is yet to be brought out.
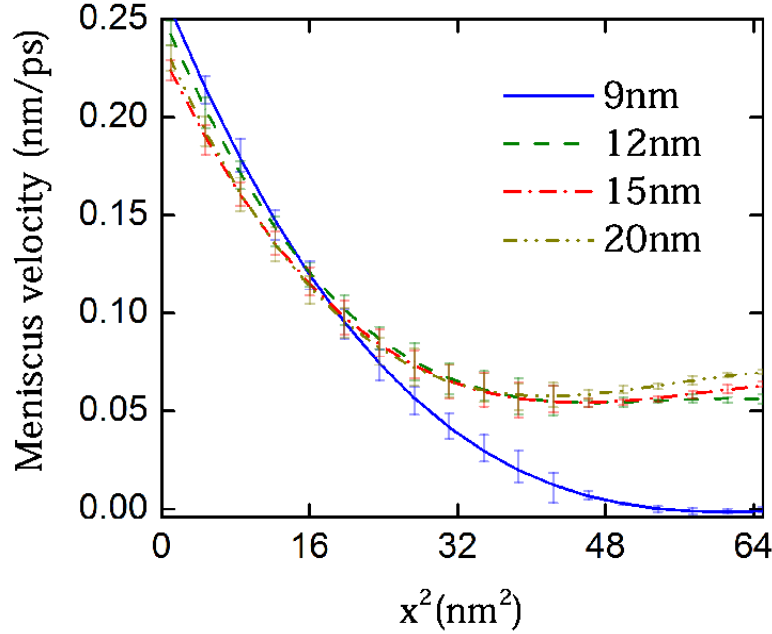
Figure 3. Comparison of filling rates for closed capillaries with the plug placed at different locations. The velocity of the meniscus front is plotted as a function of the square of the meniscus height. The observation of an intermediate acceleration to the meniscus made in Fig 2 is reinforced. The profiles have been smoothened to remove statistical fluctuations. The filtered profiles clearly depict successive attaining of velocity maxima according to the capillary length.

Theoretical Model

We begin with a reduced order model that attempts to capture the essential physics of interest in LW skeleton of filling dynamics, albeit considering a single fluid in an open-ended capillary, augmented with the Bosanquet's analysis[8,9,37]:

$$\rho \pi R^2 \frac{d}{dt}\left(x \frac{dx}{dt}\right) + 8 \pi \eta x \frac{dx}{dt} = 2 \pi R \gamma \cos \theta$$

(1)

where ρ and η are liquid density and viscosity respectively, γ is surface tension at the interface, R is the capillary radius, and θ is the equilibrium contact angle. The instantaneous average meniscus height, at any time instant t is given by x. This one-dimensional approach equates the instantaneous liquid momentum and the viscous force experienced by the imbibing fluid,

obtained by assuming a fully developed Poiseuille flow model inside the capillary, to the traction force provided by the Laplace pressure drop across the liquid-vapor interface.

We next incorporate the contribution of the gas phase to the above equation, pertinent to a closed end capillary. Towards this, we first accommodate the momentum of the gas phase and the viscous resistance offered by the gas phase, by assuming a hypothetical length scale x_g over which the gas in the capillary pore senses the meniscus motion [33]:

$$\rho\pi R^2 \frac{d}{dt}\left(x\frac{dx}{dt} \right) - \rho_g\pi R^2 \frac{d}{dt}\left(x_g\frac{dx_g}{dt} \right) + 8\pi\eta x\frac{dx}{dt} - 8\pi\eta_g x_g\frac{dx_g}{dt} = 2\pi R\gamma\cos\theta \qquad (2)$$

Here ρ_g and η_g are gas density and gas viscosity respectively. This, however, is not a complete representative of the actual physical scenario, since additional interfacial interactions at the contact line over reduced length scales need to be appropriately embedded in the above equation. The contact line force can be expressed in several forms; modified viscosity or surface tension, stick-slip length[14,48], meniscus friction[49] etc. Here, we choose to employ the meniscus friction approach [44, 45] which captures the essential physics with minimal mathematical complexity. Accordingly, we add the following term to the left hand side of Eq. (2) [50]:

$$F_{fr} = 2\pi R\chi\eta\frac{dx}{dt} \qquad (3)$$

where the meniscus friction coefficient χ depends on the properties of the three-phase contact line through the disjoining pressure isotherm[50–53]. Thus, the final equation is written as

$$\rho\pi R^2 \frac{d}{dt}\left(x\frac{dx}{dt} \right) - \rho_g\pi R^2 \frac{d}{dt}\left(x_g\frac{dx_g}{dt} \right) + 8\pi\eta x\frac{dx}{dt} - 8\pi\eta_g x_g\frac{dx_g}{dt} + 2\pi R\chi\eta\frac{dx}{dt} = 2\pi R\gamma\cos\theta \quad (4)$$

For a closed end capillary, one may substitute x_g with $L-x$, to yield:

$$R^2 \frac{d}{dt}\left[\rho x\frac{dx}{dt} + \rho_g\left(L-x \right)\frac{dx}{dt} \right] + 8\left[\eta x\frac{dx}{dt} + \eta_g\left(L-x \right)\frac{dx}{dt} \right] + 2R\chi\eta\frac{dx}{dt} = 2R\gamma\cos\theta \qquad (5)$$

11

where L is the pore length of the capillary. . Further, we may assume that $\rho_g \quad \rho$ and

$\eta_g \quad \eta$ which is true for most of the practical cases. Thus, Eq. (5) reduces to

$$R^2 \frac{d}{dt}\left(\rho x \frac{dx}{dt} + \rho_g L \frac{dx}{dt}\right) + 8\left(\eta x \frac{dx}{dt} + \eta_g L \frac{dx}{dt}\right) + 2R\chi\eta \frac{dx}{dt} = 2R\gamma \cos\theta \tag{6}$$

Integrating (6) with initial conditions $x = 0$ and $\dfrac{dx}{dt} = 0$ at $t = 0$ gives

$$R^2 \left(\rho x \frac{dx}{dt} + \rho_g L \frac{dx}{dt}\right) + 4x\left(\eta x + 2\eta_g L\right) + 2R\chi\eta x = 2R\gamma \cos\theta t \tag{7}$$

Further, substitution of our simulation parameters in Eq. (7) lead to negligible inertial effects, so that one may write

$$2x\left(\eta x + 2\eta_g L\right) + R\chi\eta x = R\gamma \cos\theta t \tag{8}$$

This, on solving, for a constant value of the friction parameter, yields

$$\frac{x}{R} = \sqrt{\left(\alpha + \chi/4\right)^2 + \frac{\gamma \cos\theta t}{2\eta R}} - \left(\alpha + \chi/4\right) \tag{9}$$

where $\alpha = \dfrac{\eta_g L}{\eta R}$. On substituting $\alpha = 0$ and $\chi = 0$ in the above equation, we get back the

original LW form.

The above equation, considering χ to be a single valued function of the static contact angle, would indicate trivial meniscus retardation in closed end capillaries, as compared to open-ended ones. However, the same may not be a complete representative of the prevailing physical scenario. This may be attributed to the fact that the friction force in a closed capillary system is not only a function of intrinsic wettability as in an open capillary pore, but also is likely to be a function of the plug distance (i.e., the total length of the channel) that dictates the action of molecules being reflected at the plug, thereby altering the behavior of three phase contact line. We, therefore, move on to describe the form of χ in absence and presence of the plug, and the implication of the same towards altering the capillary filling dynamics.

Towards this, one may first note that the mass transfer occurring at the fluid front, and the pressure changes due to it, has a characteristic time scale longer than time scale of establishing local mechanical equilibrium between the liquid and the vapor phases at the interface[51]. This, when upscaled, transcribes to the phenomenon of pinning-depinning. In other words, many cycles of liquid-gas rearrangement precede an avalanche of the fluid in the capillary pore. This rearrangement generates the disjoining pressure which counter-balances the capillary force and the meniscus remains pinned until the meniscus perceives an increased pressure on the liquid side due to accumulation of the molecules corresponding to the high-density phase at the interface. Drawing a simple dynamical analogy, we can say that the disjoining pressure or the pressure deficit at the meniscus acts akin to a friction force at the time scale of hydrodynamic pressure changes. The molecular phenomenon of fluid-vapor rearrangement, being of a shorter time scale, cannot be directly plugged in (8); however, disjoining pressure in the form of a friction force can accommodate the effect of gas layer adjoined to the interface on the meniscus dynamics, which, in turn, depends on the local interfacial film thickness.

At the molecular level, the notion of such a film boils down to a spike in the molecular number density near the wall, and the molecules do not have an identity of the phase in which they exist. Here the definition of the local film thickness h combines molecules both from displaced phase and the imbibing phase, and can be roughly estimated to be scaling with the distance of the molecular density peak from the wall. Interestingly, we observe that for closed capillary systems, the location of the number density peaks remains unaltered with changes in intrinsic substrate wettability. Thus, we conclude that while for an open capillary system the meniscus friction is a strong function of wettability, for closed capillary system the meniscus friction becomes a strong function of the thickness of the leading film or the concentration of the species just ahead of the meniscus rather than the wettability of the surface. Thus with a plug in front of the capillary (i.e., a closed end capillary), the value of h becomes invariant with the intrinsic contact angle of the substrate. Also, we observe that the location of the density peak for closed pores is quite similar to that of a completely wettable open pore, irrespective of the intrinsic wettability of the closed pore. As the film thickness strongly dominates the contact line friction, we can conclude that the contact line friction becomes independent of the wettability of the substrate for a closed capillary. With this knowledge, the dynamics of any closed capillary can be derived from (8) as

$$2x\left(\eta x + 2\eta_g L\right) + R\chi_0 \eta x = R\gamma \cos\theta t \tag{10}$$

where χ_0 is the meniscus friction coefficient for a completely wettable open capillary pore. We infer that although, at a lower wettability in a closed capillary, the meniscus traction force is lower owing to the decrease in surface tension force, the meniscus friction force is lower (equal to a completely wettable pore) and thus the compensating viscous force would need a larger meniscus velocity and hence, the accelerated filling rates. We elaborate this in the next section where we compare open and closed capillaries of different wettabilities and validate our hypothesis by comparing it with the MD results.

Comparison with MD Simulations

In order to delve deeper into the physics of meniscus formation and propulsion through nano-capillary pores in presence of a trapped gas phase, we simulate capillary filling through open and closed capillaries of different wettabilities and compare the MD simulation predictions with the corresponding theoretical predictions. To impart visual ease to the comparison, we plot the square of the local filling length with time, both in reduced units (see Fig. 4). For the closed capillary simulations, the plug is placed at a distance of $15nm$ from the capillary pore entrance. The dynamics of the meniscus is shown for the first $2ns$ during which the meniscus level remains at a considerable distance from the plug in order to avoid the dynamics of direct flow choking by the plug. We deliberately make this choice to ensure the meniscus, even for the completely wettable case, remains at a distance greater than van der Waals cut-off from the plug[46].

Several interesting features are revealed from Fig. 4. First, for completely wettable capillary pores, the difference in meniscus dynamics for closed and open capillaries is negligible. Although the velocities might be different during the filling process, the integral distance traversed by the meniscus does not show any discernable difference between the open and closed cases. Since, the studies previously attempted most of the times dealt with completely wettable capillaries, the retardation of capillary flow due to enhanced viscous force of the entrapped gas layer was only observed[33]. However, non-intuitive results may be obtained as we reduce the

wettability of the capillary walls and compare the data obtained for closed and open channels. The rate of filling of capillaries of lower wettability shows appreciable increase for the closed capillaries as compared to the open ones. This observation is completely counter-intuitive and is in direct opposition to the macro-scale results for closed capillary systems[33–38]. The closed capillaries with intermediate wettability values (a representative result shows a capillary with walls having contact angle of 46°) show a slight increase in filling rate, however, capillaries which have walls with further less intrinsic wettability (contact angle approaching 90°) depict a tremendous instantaneous increase in the filling rates. We illustrate this behavior for an intrinsic contact angle of 72°.
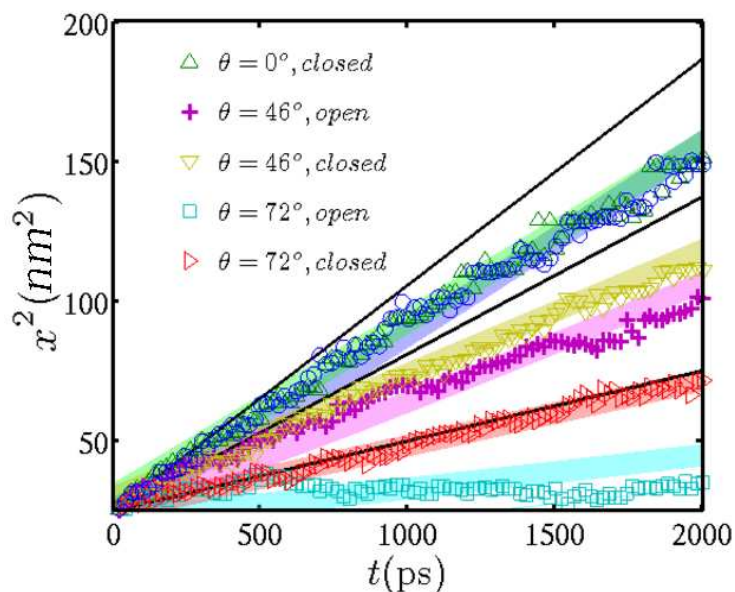

Figure 4. Comparison of meniscus filling for open and closed capillaries of different intrinsic wettabilities. While, the filling rate remains almost the same for completely wetting capillary walls, it increases for partially wetting walls and registers larger increase for walls with lower wettability values. The shaded lines depict the results of the LW equation extended with the contact line friction term. For open pores, the meniscus friction coefficient has been determined by simulating droplet motion. In particular, we execute droplet-based simulations on surfaces similar to the capillary walls considered here and artificially tune the ambient humidity of the droplet[54,55]. For closed pores, the same is obtained as an extension to completely wettable open pores (for details see text).

A closer observation of Fig. 4 reveals yet another interesting phenomenon. The filling rates for both open and closed capillaries with a particular wettability remain the same at the initial stages of filling. The rates of filling for closed capillaries start taking off after a certain time has elapsed. Again, the time at which this filling rate 'take-off' occurs is more for more wettable capillaries. For example, for contact angle of 46°, the closed capillary filling rate 'take-off' occurs at around 1100 time units, whereas for contact angle of 72° that occurs around 700 time units. Thus, there occurs an intermediate temporal regime over which an intrinsically less wettable channel exhibits augmented filling rates as compared to an otherwise intrinsically more wettable channel. This indicates that the presence of the plug would thwart the effect of hydrophobicity. Lesser wettability of the walls in a closed capillary seems to increase the driving force propelling the liquid in the meniscus. In all cases, there is a very good agreement between the MD predictions and the theoretical model predictions, within an error bar of $\pm 5\%$.

Discussions

The results shown above clearly indicate that the plug has a two-way effect on the meniscus motion. At a distance greater than the range of van der Waals force, the plug aids the ascent of fluid in the capillary; however, within the van der Waals force range, the plug begins to retard the progress of the meniscus. The process of meniscus retardation is well understood and occurs due to the increased resistance offered by the gas molecules that are being progressively compressed between the meniscus and the plug[33–38]. On the other hand, the initial speeding up of the meniscus signals at some phenomenon which is yet to be brought to light.

In an effort to bring out the above, we note that the plug in a closed capillary interferes with the pinning-avalanche phenomenon occurring at the meniscus. The plug acts as a concentrator and reflector of the molecules in the gas phase which helps to augment the contact angle at the meniscus, and aids in reaching the advancing contact angle value faster. The effect of the plug is observed to be more pronounced in cases of lower intrinsic wettability. Since, the meniscus moves forward more favorably by evaporation-condensation rather than surface diffusion for capillaries having lower intrinsic wettability, the presence of the plug dramatically increases the probability of gas molecules condensing back to the meniscus zone and leads to faster occurrences of pinning-avalanche cycles. The plug alters the gas concentration and dynamics in the confined zone above the meniscus. This, in turn alters the pinning and depinning

16

of the meniscus. For a completely wettable pore, a prewetting film spreads rapidly ahead of the meniscus leading to minimum contact angle hysteresis. Pores having lower wettability, however, are expected to have greater contact angle hysteresis and the intrinsically lower filling rates of capillary with prolonged pinning phases in between. The presence of plug, in such a case, accelerates the pinning-depinning cycle on account of the increased number of molecules moving into the gas phase due to lower pore wettability. Thus, with a plug there is a two-way increase in the filling rates of pores of lower wettability. Firstly, compared to the open pore the closed pore enhances the depinning of the meniscus and secondly, the increased number of gas molecules due to lower wettability again serves as a precursor for movement of meniscus via diffusion. We observe the same in Fig. 4, where the filling rate for a capillary with contact angle of 72^0 for pure water shows colossal increase as compared to the open capillary case upon introduction of the plug. The take-off in the filling rates of the closed capillaries occurs when the particles in the gas phase start interacting with the plug. The lower the intrinsic wettability of the capillary walls, the more would be the escape of molecules into the gas phase and hence, the take-off would occur at an earlier stage. The combined effect of hydrophobicity and the presence of plug increases the gas concentration near the meniscus and hence results in a faster capillary rise.

For higher values of the static contact angle, the film ahead of the imbibing fluid is not rich in molecules; however, the interfacial gas phase has more molecules owing to substrate hydrophobicity. On the other hand, substrates with lower static contact angle values have an extended film which compensates the poor concentration of trapped gas molecules. This implies that a closed capillary would have a constant meniscus friction coefficient irrespective of the intrinsic wettability. With this hypothesis, one may equate the value of the meniscus friction coefficient of a completely wettable closed pore to that of a completely wettable open pore (assuming completely wettable pores lead to instantaneous film formation ahead of the meniscus as soon as the meniscus is formed at the interface) and substitute the same value in Eq. (9) for pores with different contact angles. The above conceptual paradigm has been verified by nice agreement between our theoretical predictions and MD predictions.

Conclusions

Using a comparison between the interfacial phenomena characterizing the meniscus dynamics in open and closed capillaries of nanoscopic length scales under similar conditions, we demonstrate through MD simulations that the existence of a closed end does not trivially oppose the fluid filling in the capillary, but may also accelerate the rate of filling over an intermediate temporal regime. We attribute the same to the physics of meniscus formation and pinning-depinning mechanism over nanometer length scales. This, in turn, offers with a possibility of accelerating the capillary filling rate in nanopores, by realizing interplay of dynamical interactions between the displacing and the displaced phase towards altering the interfacial friction. This opens several prospects in natural systems, for example, in oil recovery systems in which closed end nanocapillaries are omnipresent. Interestingly, the presence of a closed end enhances the instantaneous throughput for a partially wettable system more than a completely wettable system and this property can be used in many industrial purposes.

Notes and references

Department of Mechanical Engineering, Indian Institute of Technology Kharagpur, Kharagpur 721302, INDIA

*E-mail: suman@mech.iitkgp.ernet.in

1.   J. Boreyko and C.-H. Chen, *Phys. Rev. Lett.*, 2009, **103**, 184501.

2.   G. R. Willmott, C. Neto, and S. C. Hendy, *Soft Matter*, 2011, **7**, 2357.

3.   P. Abgrall and N. T. Nguyen, *Anal. Chem.*, 2008, **80**, 2326–41.

4.   S. Darwich, K. Mougin, and H. Haidara, *Soft Matter*, 2012, **8**, 1155.

5.   D. Lohse, *Phys. Today*, 2003, **56**, 36–41.

6.   H.-Q. Sun, L. Zhang, Z.-Q. Li, L. Zhang, L. Luo, and S. Zhao, *Soft Matter*, 2011, **7**, 7601.

7.   X. Li, X. Ma, D. Fan, and C. Zhu, *Soft Matter*, 2012, **8**, 3781.

8.   R. Lucas, *Kolloid-Zeitschrift*, 1918, **23**, 15–22.

9.   E. W. Washburn, *Phys. Rev.*, 1921, **17**, 391–283.

10.   X. Xu and T. Qian, *Phys. Rev. E*, 2012, **85**, 1–17.

11.   S. Granick, Y. Zhu, and H. Lee, *Nat. Mater.*, 2003, **2**, 221–7.

12.   J. Janecek and R. R. Netz, *Langmuir*, 2007, **23**, 8417–29.

13.   M. Nosonovsky, *Nature*, 2011, **477**, 412–3.

14.   C. Bakli and S. Chakraborty, *Appl. Phys. Lett.*, 2012, **101**, 153112.

15.   D. Quéré, *Annu. Rev. Mater. Res.*, 2008, **38**, 71–99.

16.   A. Niavarani and N. V. Priezjev, *Phys. Rev. E*, 2010, **81**, 1–10.

17.   T. M. Galea and P. Attard, *Langmuir*, 2004, **20**, 3477–3482.

18.   B. Xu, Y. Li, T. Park, and X. Chen, *J. Chem. Phys.*, 2011, **135**, 144703.

19.   D. Ebert and B. Bhushan, *J. Colloid Interface Sci.*, 2012, **368**, 584–91.

20.   A. Vadakkepatt, Y. Dong, S. Lichter, and A. Martini, *Phys. Rev. E*, 2011, **84**, 1–11.

21.   N. Fries and M. Dreyer, *J. Colloid Interface Sci.*, 2009, **338**, 514–8.

22.   M. Hilpert, *J. Colloid Interface Sci.*, 2009, **337**, 131–7.

23.   G. Martic, F. Gentner, D. Seveno, D. Coulon, J. De Coninck, and T. D. Blake, *Langmuir*, 2002, **18**, 7971–7976.

24.   G. Martic, T. . D. Blake, J. De Coninck, and J. D. Coninck, *Langmuir*, 2005, **21**, 11201–11205.

25.   S. Chakraborty, D. Chatterjee, and C. Bakli, *Phys. Rev. Lett.*, 2013, **110**, 184503.

26.   L. Joly, C. Ybert, E. Trizac, and L. Bocquet, *Phys. Rev. Lett.*, 2004, **93**, 1–4.

27.   C. Bouzigues, P. Tabeling, and L. Bocquet, *Phys. Rev. Lett.*, 2008, **101**.

28.   L. Joly, C. Ybert, E. Trizac, and L. Bocquet, *J. Chem. Phys.*, 2006, **125**, 204716.

29.   C. Chen, L. Zhuang, X. Li, J. Dong, and J. Lu, *Langmuir*, 2012, **28**, 1330–6.

30. Y. Chen, J. Weng, J. R. Lukes, A. Majumdar, and C.-L. Tien, *Appl. Phys. Lett.*, 2001, **79**, 1267.

31. E. B. Dussan V. and S. H. Davis, *J. Fluid Mech.*, 2006, **65**, 71.

32. V. Ludviksson and E. N. Lightfoot, *AIChE J.*, 1968, **14**, 674–677.

33. M. Hultmark, J. M. Aristoff, and H. A. Stone, *J. Fluid Mech.*, 2011, **678**, 600–606.

34. F. Chauvet, S. Geoffroy, A. Hamoumi, M. Prat, and P. Joseph, *Soft Matter*, 2012, **8**, 10738.

35. A. V. Pesse, G. R. Warrier, and V. K. Dhir, *Int. J. Heat Mass Transf.*, 2005, **48**, 5150–5165.

36. B. V. Zhmud, F. Tiberg, and K. Hallstensson, *J. Colloid Interface Sci.*, 2000, **228**, 263–269.

37. C. H. Bosanquet, *Philos. Mag. Ser. 6*, 1923, **45**, 525–531.

38. R. Fazio and S. Iacono, *Proc. World Congr. Eng.*, 2009, **WCE 2009 V**.

39. D. Schneider, R. Valiullin, and P. A. Monson, *Langmuir*, 2014, **30**, 1290–4.

40. H. Lim, A. Tripathi, and J. Lee, *Langmuir*, 2014.

41. V. N. Phan, N.-T. Nguyen, C. Yang, P. Joseph, L. Djeghlaf, D. Bourrier, and A.-M. Gue, *Langmuir*, 2010, **26**, 13251–5.

42. F. B.-W. P.-G. de Gennes, *Capillarity and Wetting Phenomena: Drops, Bubbles, Pearls, Waves*, Springer, New York, 2003.

43. A. Martini, H. Hsu, N. A. Patankar, and S. Lichter, *Phys. Rev. Lett.*, 2008, **206001**, 1–4.

44. P. Thompson and M. Robbins, *Phys. Rev. Lett.*, 1989, 63, 766–769.

45. H. J. C. Berendsen, J. R. Grigera, and T. P. Straatsma, *J. Phys. Chem.*, 1987, **91**, 6269–6271.

46. M. . Allen and D. . Tildesley, *Computer Simulation of Fluids*, Clarendon Press, 1987.

47. N. R. Tas, J. Haneveld, H. V. Jansen, M. Elwenspoek, and A. van den Berg, *Appl. Phys. Lett.*, 2004, **85**, 3274.

48. L. Joly, *J. Chem. Phys.*, 2011, **135**, 214705.

49. a Hamraoui, *J. Colloid Interface Sci.*, 2000, **226**, 199–204.

50.   T. Andrukh, D. Monaenkova, B. Rubin, W.-K. Lee, and K. G. Kornev, *Soft Matter*, 2014, **10**, 609.

51.   K. Kornev, A. Neimark, and A. Rozhkov, *Adv. Colloid Interface Sci.*, 1999, **82**, 127–187.

52.   K. Kornev and G. Shugai, *Phys. Rev. E*, 1998, **58**, 7606–7619.

53.   A. G. Egorov, K. G. Kornev, and A. V. Neimark, *Phys. Fluids*, 2003, **15**, 3134.

54.   M. J. de Ruijter, T. D. Blake, and J. De Coninck, *Langmuir*, 1999, **15**, 7836–7847.

55.   A. Balankin, H. Zapata López, E. Pineda León, D. Morales Matamoros, L. Morales Ruiz, D. Silva López, and M. Rodríguez, *Phys. Rev. E*, 2013, **87**, 014102.